

Time-dependent and Time-independent Directional Search for High-Energy Astrophysical Neutrino Point Sources in Super-Kamiokande

Xubin Wang^{a,*} for the Super-Kamiokande Collaboration

^a*Research Center for Cosmic Neutrinos, Institute for Cosmic Ray Research, University of Tokyo
Kashiwa, Chiba 277-8582, Japan*

E-mail: wang-xubin20@g.ecc.u-tokyo.ac.jp

This contribution reports the results of the searches for high-energy astrophysical neutrino point sources in the energy range above GeV using Super-Kamiokande data. The searches include time-integrated and time-dependent full sky searches for both ν_μ and ν_e sources and coincidence check with candidates including TXS 0506+056 and NGC 1068. The searches use unbinned maximum likelihood method, and test statistics is calculated to find signal excess over atmospheric neutrino background. The time-integrated search method is updated from a previous search by adding the neutrino energy distribution in the likelihood to consider different power-law emission spectra with varying spectral indices. This is the first time to perform the time-dependent search, which has a better performance in searching for neutrino emission in a short time period, in Super-Kamiokande. Upper limits on neutrino flux or fluence are set for all searches.

38th International Cosmic Ray Conference (ICRC2023)
26 July - 3 August, 2023
Nagoya, Japan



*Speaker

1. Introduction

We have observed ultra-high energy cosmic rays with energies up to 10^{20} eV in our advanced experiments, yet the origin of them is still unknown to us. Such cosmic rays are considered to have been accelerated after their production via certain kind of acceleration mechanism. Neutrino is ideal for studying the source and production process of high energy cosmic rays since it is not deflected by the magnetic field and hardly interact with matter when propagating in galaxy. Since 2017, IceCube has reported several evidences of astrophysical high energy neutrinos observation from sources including blazar TXS 0506+056 and active galaxy NGC 1068 in TeV range [1–3]. Super-Kamiokande (SK) is sensitive in GeV range to both muon neutrino ν_μ and electron neutrino ν_e and has visibility to to all sky, and has been running for more than 20 years with a low dead-time ratio. This proceedings presents the results of searches for astrophysical high energy neutrino point sources using all SK data recorded during SK phases before Gadolinium loading. In this analysis, we updated the 11-year point source search in SK [4] and improved the searching method by extending the search to all high-energy samples and two neutrino flavors, and taking into account different emission energy spectrum. We also established the searching method and performed the time-dependent search for the first time in SK.

2. Super-Kamiokande and Data Sample

Super-Kamiokande is a water Cherenkov detector with 50kt ultra-purified water and has an inner detector (ID) and an outer detector (OD). High-energy neutrino events in SK are categorized into three samples based on topology: fully contained (FC), partially contained (PC) and upward-going muon (UPMU). The reconstructed neutrino interaction vertices are inside the inner detector for both FC and PC events. Events with all daughter events stops within the ID are classified as FC, while those have energy deposited in the OD are classified as PC. UPMU are muons traveling upward coming below the horizon, created by the neutrinos interacting with the water or rock surrounding the detector. The angular resolution becomes better as the energy of event gets larger, so an minimum energy threshold is applied on each sample to have angular resolution compatible with 15° searching region used in the searches. This threshold is set to 2.3 GeV for FC, 1 GeV for PC and 1.6 GeV for UPMU. All three samples are sensitive to ν_μ , and they are all used in the search for ν_μ astrophysical point source. FC and PC are also sensitive to ν_e , but we only use FC for the search for ν_e point source as only a negligible amount of ν_e in PC are left above the energy threshold. In the ν_μ (ν_e) point source search, all FC events will be treated as ν_μ (ν_e) events. The searches use the data of all five SK water operation phases from SK-I to SK-V taken from April 1996 to May 2019 with a total live time of 6511 days, including 7940 FC, 3859 PC and 9389 UPMU events.

3. Search Method

We are searching for both a spatial clustering of high energy neutrinos during the whole running period from SK-I to SK-V in time-integrated search, and a both temporal and spatial clustering in a shorter time in time-dependent search. In both of the searches, we use the unbinned maximum

likelihood method, and the likelihood is given as the follow:

$$\mathcal{L} = \frac{e^{-(n_S+n_B)}(n_S+n_B)^N}{N!} \prod_j \prod_{i \in j} \left(\frac{n_S}{n_S+n_B} S_{j,i} + \frac{n_B}{n_S+n_B} B_{j,i} \right) \quad (1)$$

where j is the sample (FC, PC or UPMU), n_S and n_B are the total expected number of signal and background events of all three samples, respectively, N is the total number of observed events within the 15° searching region around the searching direction, $S_{j,i}$ and $B_{j,i}$ are the signal PDF and background PDF of the i^{th} event in sample j . In time-integrated search

$$S_{j,i} = \mathcal{A}_{s,i}^{sig}(\Delta\phi_{j,i}|E_{j,i})\mathcal{E}_{j,i}^{sig}(E_{j,i}|\gamma)\mathcal{M}_j^{sig}(\gamma) \quad (2)$$

$$B_{j,i} = \mathcal{A}_{s,i}^{bkg}(\delta_{j,i}|E_{j,i})\mathcal{E}_{j,i}^{bkg}(E_{j,i})\mathcal{M}_j^{bkg} \quad (3)$$

Here $\mathcal{A}_{s,i}^{sig}$ and $\mathcal{E}_{s,i}^{sig}$ are the signal angular and energy PDF. $\mathcal{M}_j^{sig}(\gamma)$ is the probability for a signal event with energy spectrum γ to be detected as sample j , and \mathcal{M}_j^{bkg} is the fraction of number of background events for sample j . All of these above are simulated using Monte Carlo (MC). $\Delta\phi_i$ is the angle between the searching direction and the reconstructed direction, E_i is the reconstructed energy, δ_i represents declination in equatorial coordinate (J2000) of the event. For time-dependent search:

$$S_{j,i} = \mathcal{A}_{s,i}^{sig}(\Delta\phi_{j,i}|E_{j,i})\mathcal{E}_{j,i}^{sig}(E_{j,i}|\gamma)\mathcal{M}_j^{sig}(\gamma)\mathcal{T}_i^{sig}(t_{j,i}|t_0, \sigma_t) \quad (4)$$

$$B_{j,i} = \mathcal{A}_{s,i}^{bkg}(\delta_{j,i}|E_{j,i})\mathcal{E}_{j,i}^{bkg}(E_{j,i})\mathcal{M}_j^{bkg}\mathcal{T}^{bkg} \quad (5)$$

Here $\mathcal{T}_i^{sig}(t_{j,i}|t_0, \sigma_t)$ is a Gaussian distribution function while \mathcal{T}^{bkg} is a constant assuming uniform distribution over all SK-I to SK-V running time. $t_{j,i}$ is the detection time of the event and t_0 and σ_t being emission center time (Gaussian mean time) and emission time duration (Gaussian standard error). The rest are the same as in time-integrated search, except that δ_i in $\mathcal{A}_i^{bkg}(\delta_i|E_i)$ is the altitude in detector coordinate. Number of signal events n_S and energy spectrum γ are free parameters to be fitted to maximize the likelihood in both time-integrated and time-dependent search. Time-dependent search has two extra free parameters, t_0 and σ_t . Then we evaluate the significance of the hypothesis of having \hat{n}_S events against the null hypothesis by calculating the test statistics:

$$TS = 2 \log \left[\frac{\mathcal{L}(\hat{n}_S)}{\mathcal{L}(n_S = 0)} \right] \quad (6)$$

where \hat{n}_S is the best fitted n_S . In time-dependent search, an extra term is added to include the effect of look else-where (trial factor)[5], and the final test statistics is:

$$TS = 2 \log \left[\frac{\hat{\sigma}_t}{T_{tot}} \times \frac{\mathcal{L}(\hat{n}_S)}{\mathcal{L}(n_S = 0)} \right] \quad (7)$$

where \hat{t}_0 is the best fitted t_0 and T_{tot} is the total live time from SK-I to SK-V. In total we performed four individual full-sky searches: time-integrated search and time-dependent search, for ν_e and ν_μ astrophysical point source. In the full-sky search the sky is divided into 49152 equal-area pixels using the HEALPix method[7] and the center of each pixel is used as one searching direction. We fit free parameters n_S , γ , t_0 and σ_t , and calculate the test statistics and pre-trial p-value for all

searching directions, and pick out the direction with maximum TS (called the best fitted direction) in the sky. In order to evaluate the significance of this result, we calculate the pre-trial p value and post-trial p value. Pre-trial p value is fraction of TS at the same declination simulated from pseudo-experiments (trials) with solely background toy MC that maximum TS from the data is larger than. Definition for post-trial p value is similar to pre-trial p value, with the overall maximum TS in the whole sky replacing TS at the same declination. Trial factor has been included in the post-trial p value. With smaller p value, we have more confidence in this being an astrophysical point source instead of background fluctuation. If no significant excess is found, we will set an upper limit on the neutrino flux (for time-integrated search) or fluence (for time-dependent search) in that direction. For time-integrated search, the neutrino flux is averaged over the total live time from SK-I to SK-V. This neutrino flux and fluence are the integrated flux and fluence from 1 GeV to 10^5 GeV with spectral index being the optimized one from that search.

The sensitivities, which is defined as the number of signal events needed so that 50% of the maximum TS of trials is larger than 90% of maximum TS of trials with solely background toy MC, for each search, and converted the sensitivities in terms of neutrino flux or fluence. The results of the sensitivities are shown in Figure 1. There is no UPMU event for declination above 53.6° as no UPMU comes above the horizon in the detector coordinate. The sensitivity in time-integrated search for ν_μ becomes much worse if the searching region overlaps with the region above 53.6° , so only sensitivity below 40° is presented. Sensitivity for ν_μ search below 53.6° is much better than that above 53.6° and that for ν_e due to the difference of the effective area, as shown in Figure 2.

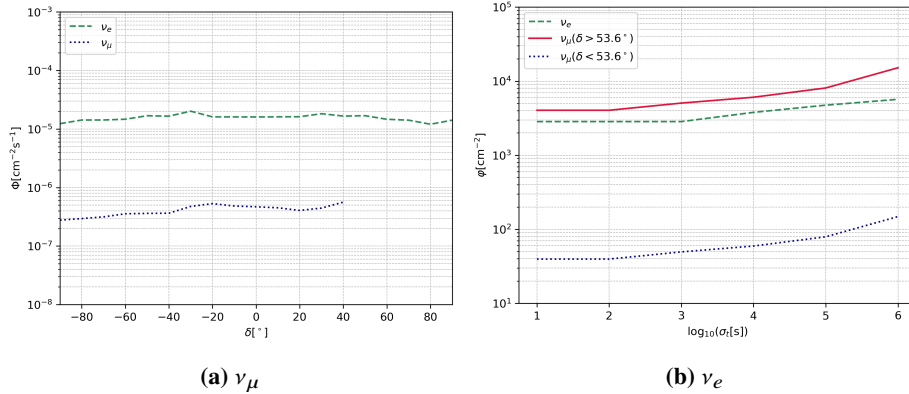


Figure 1: The sensitivities in terms of neutrino flux in time-integrated search (a) for ν_μ (blue dotted line) and ν_e (green dashed line) for different declination, and in terms of neutrino fluence time-dependent search (b) for ν_μ below 53.6° (blue dotted line), above 53.6° (red solid line) and for ν_e (green dashed line) for different assumed emission duration σ_t . The neutrino flux and fluence are integrated from 1 GeV to 10^5 GeV assuming $\gamma = 2$.

4. Results

4.1 Time-Integrated Search

Figure 3 show the sky maps of TS for the time-integrated search for ν_μ and ν_e . The best fitted direction are found at right ascension and declination of $(\delta = 296.3^\circ, \alpha = -81.2^\circ)$ and

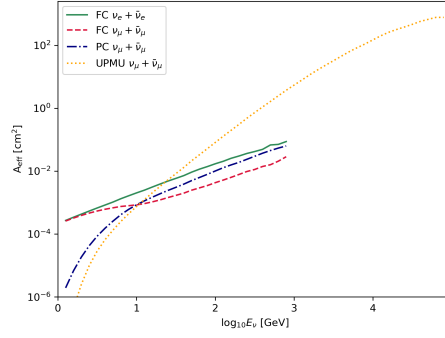


Figure 2: Effective area for FC ν_e (green solid line), FC ν_μ (red dashed line), PC ν_μ (blue dashdot line) and UPMU ν_μ (yellow dotted line) as a function of log of neutrino energy. This figure is recreated using the data from [6].

($\delta = 245.1^\circ$, $\alpha = -48.1^\circ$) in search for ν_μ and ν_e , respectively. The events distributed around these best fitted direction are shown in Figure 4. The TS at the best fitted direction in the search for ν_e stands out among all searching directions since it is close to an event with energy up to 140.6 GeV, which is one of the events with highest energies. Astrophysical neutrino is expected to have a softer energy spectrum compared with atmospheric neutrino, thus high energy event is more likely to be an astrophysical neutrino than an atmospheric neutrino. The pre-trial p values are 2.7×10^{-4} for the search for ν_μ , corresponding to a post-trial p value of 94.0%, and 4.5×10^{-3} for ν_e , with corresponding post-trial p value of 99.2%. No significant excess with respect to background was found in either search according to the p values, so 90% confidence level upper limit was set on the neutrino flux to $\Phi^{90\text{CL}} = 6.0 \times 10^{-7} [\text{cm}^{-2}\text{s}^{-1}]$ and $\Phi^{90\text{CL}} = 3.4 \times 10^{-6} [\text{cm}^{-2}\text{s}^{-1}]$ for the search for ν_μ and ν_e , respectively. The results are summarized in Table 1.

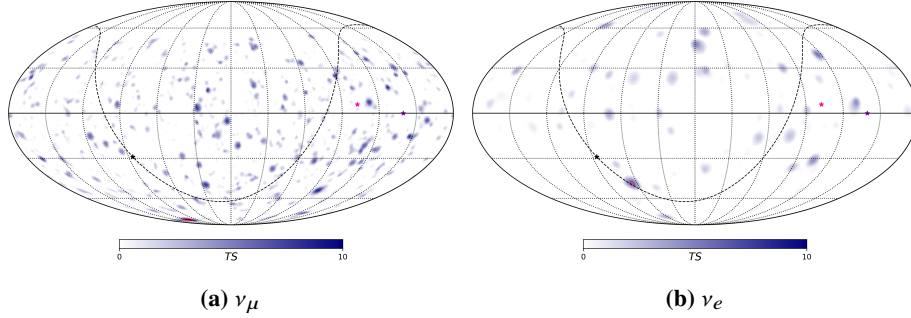


Figure 3: Sky map of TS in time-integrated search for ν_μ (a) and ν_e (b). The best fitted direction is indicated by red circle. Dashed line and black star on it represent galactic plane and galactic center. TXS 0506+056 and NGC 1068 are indicated by pink and purple star.

4.2 Time-Dependent Search

The sky maps of TS is shown in Figure 5 for the time-dependent search for ν_μ and ν_e . The best fitted direction are found at ($\delta = 121.6^\circ$, $\alpha = -30.0^\circ$) and ($\delta = 133.5^\circ$, $\alpha = 52.0^\circ$), and the best fitted emission center times are $t_0 = 55574.04\text{mjd}$ and $t_0 = 57530.28\text{mjd}$, in search for ν_μ and ν_e , respectively. Figure 6 shows the event spatial and temporal distribution around the best fitted

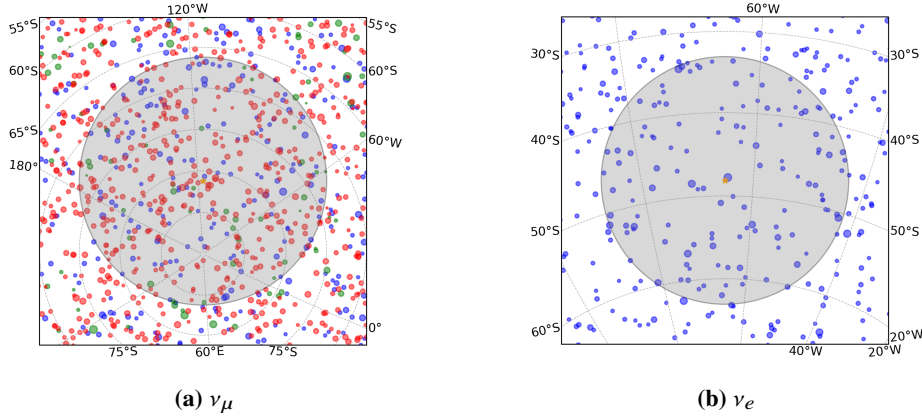


Figure 4: Events distribution around the best fitted direction in time-integrated search for ν_μ (a) and ν_e (b). Best fitted direction is indicated by yellow star in the center. Blue, green and red dots are FC, PC and UPMU events, respectively. Shaded region encircled by solid line is the search region. The size of the marker is proportional to $\log_{10} E_{vis}$.

Table 1: Best fitted number of events \hat{n}_S , energy spectrum index $\hat{\gamma}$, right ascension $\hat{\alpha}$ and declination $\hat{\delta}$, pre-trial p value, post-trial p value and neutrino flux upper limit Φ^{90CL} in the time-integrated searches for ν_μ and ν_e .

	\hat{n}_S	$\hat{\gamma}$	$\hat{\alpha}$ [°]	$\hat{\delta}$ [°]	pre p	post p	Φ^{90CL} [$\text{cm}^{-2}\text{s}^{-1}$]
ν_μ	8.4	2.1	296.3	-81.2	2.7×10^{-4}	94.0%	6.0×10^{-7}
ν_e	1.7	1.5	245.1	-48.1	4.5×10^{-3}	99.2%	3.4×10^{-6}

direction within $\hat{t}_0 \pm 3\hat{\sigma}_t$. One FC event and two UPMU events are found around the best fitted direction and best fitted emission center time within $\pm 10\text{h}$ in the search for ν_μ , and three FC events around the best fitted direction and emission center time within $\pm 6\text{h}$ in the search for ν_e . Pre-trial p value of the best fitted direction in the search for ν_μ is 1.4×10^{-3} , corresponding to a post-trial p value of 96.2%. The pre-trial p value with its corresponding post-trial p value in the search for ν_e are 7.1×10^{-4} and 82.6%. No significant excess with respect to background in either search was found according to the p values, and the 90% confidence level neutrino fluence upper limits was set to and for the searches for ν_μ and ν_e , respectively. The results of these two searches are summarized in Table 2.

Table 2: Best fitted number of events \hat{n}_S , energy spectrum index $\hat{\gamma}$, emission time duration $\hat{\sigma}_t$ and center time \hat{t}_0 , right ascension $\hat{\alpha}$ and declination $\hat{\delta}$, pre-trial p value, post-trial p value and neutrino fluence upper limit φ^{90CL} in the time-dependent search for ν_μ and ν_e .

	\hat{n}_S	$\hat{\gamma}$	$\hat{\sigma}_t$ [s]	\hat{t}_0 [mjd]	$\hat{\alpha}$ [°]	$\hat{\delta}$ [°]	pre p	post p	φ^{90CL} [cm^{-2}]
ν_μ	3.0	2.0	2.5×10^4	55574.04	121.6	-30.0	1.4×10^{-3}	96.2%	8.3×10^1
ν_e	3.0	2.5	1.4×10^3	57530.28	133.5	52.0	7.1×10^{-4}	82.6%	1.4×10^4

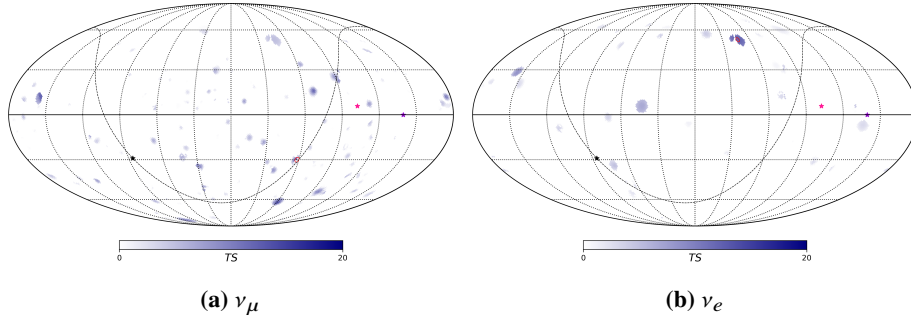


Figure 5: Sky map of TS in time-dependent search for ν_μ (a) and ν_e (b). The best fitted direction is indicated by red circle. Dashed line and black star on it represent galactic plane and galactic center. TXS 0506+056 and NGC 1068 are indicated by pink and purple star.

4.3 Check for Coincidence with Candidates

After obtaining the results of the full sky searches, we compared sky map from those results with a list of candidates including blazar TXS 0506+056, active galaxy NGC 1068, high-energy neutrino alerts from IceCube (2010-2017)[8] and sources from TeVCat catalog[9] for the coincidence check, but no significant coincidence with any candidates were found in any of the search.

5. Conclusions

The results of searches for high-energy astrophysical neutrino point sources with SK has been presented. Both time-integrated and time-dependent search for two flavors of neutrino, ν_μ and ν_e , have been performed using the data of SK water operation phases from SK-I to SK-V taken from April 1996 to May 2019 with a total live time of 6511 days including FC, PC and UPMU samples. No significant evidence of high-energy astrophysical neutrino point source has been found in any of the the four searches. The best fitted directions in time-integrated search for ν_μ have been found at $(\delta = 296.3^\circ, \alpha = -81.2^\circ)$, with pre-trial p value of 2.7×10^{-4} and corresponding post-trial p value of 94.0%, and the 90% confidence level upper limit on neutrino flux set to $\Phi^{90\text{CL}} = 6.0 \times 10^{-7} [\text{cm}^{-2}\text{s}^{-1}]$. For time-integrated search for ν_e , the best fitted direction is at $(\delta = 245.1^\circ, \alpha = -48.1^\circ)$ with pre-trial p value of 4.5×10^{-3} and corresponding post-trial p value of 99.2%, and neutrino flux upper limit set to $\Phi^{90\text{CL}} = 3.4 \times 10^{-6} [\text{cm}^{-2}\text{s}^{-1}]$. For time-dependent search for ν_μ , the best fitted direction is at $(\delta = 121.6^\circ, \alpha = -30.0^\circ)$ with pre-trial p value of 1.4×10^{-3} and corresponding post-trial p value of 96.2%, and neutrino fluence upper limit set to $\varphi^{90\text{CL}} = 8.3 \times 10^1 [\text{cm}^{-2}]$. For time-dependent search for ν_e , the best fitted direction is at $(\delta = 133.5^\circ, \alpha = 52.0^\circ)$ with pre-trial p value of 7.1×10^{-4} and corresponding post-trial p value of 96.2%, and neutrino fluence upper limit set to $\varphi^{90\text{CL}} = 1.4 \times 10^4 [\text{cm}^{-2}]$. A check for coincidence with candidates including TXS 0506+056 and NGC 1068 has also been performed with the result of each of the four searches. No significant coincidence with any candidates were found in any of the search.

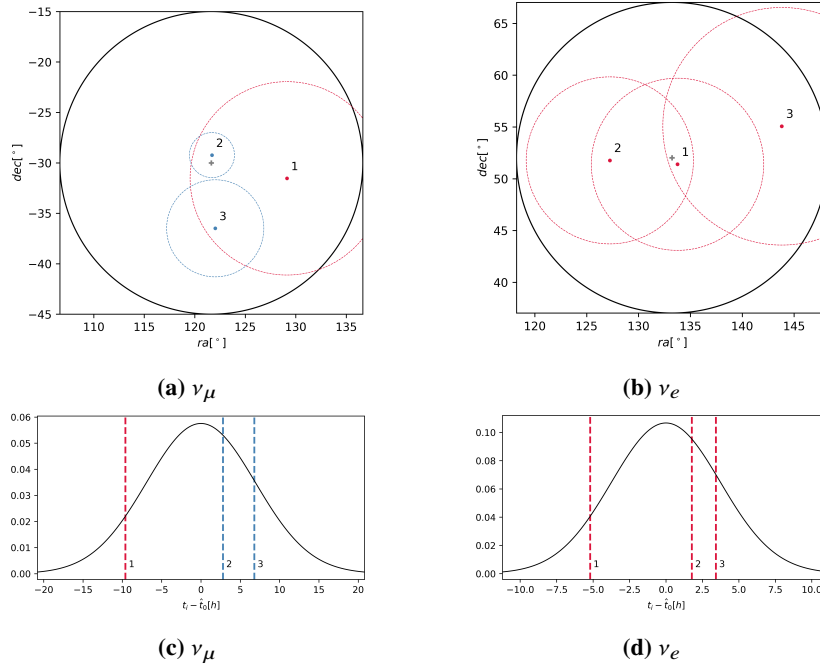


Figure 6: Top two figures: events spatial distribution around the best fitted direction in time-dependent search for ν_μ (a) and ν_e (b). Red, green and blue dots are FC, PC and UPMU events, respectively. The dashed circle indicate the angular resolution (estimated error) of each event. Black cross is the best fitted direction, and the black solid circle is the 15° search region boundary. Bottom two figures: events time distribution around the best fitted center of time in time-dependent search for ν_μ (c) and ν_e (d). Red, green and blue vertical lines are FC, PC and UPMU events, respectively. The black line indicate the Gaussian distribution given \hat{t}_0 and $\hat{\sigma}_T$.

References

- [1] IceCube Collaboration, et al., Science 361.6398 (2018): eaat1378.
- [2] IceCube Collaboration, et al., Science 361.6398 (2018): 147-151.
- [3] IceCube Collaboration, et al., Science 378.6619 (2022): 538-543.
- [4] Super-Kamiokande Collaboration, et al., The Astrophysical Journal 704.1 (2009): 503.
- [5] IceCube Collaboration, et al., The Astrophysical Journal 911.1 (2021): 67.
- [6] Super-Kamiokande Collaboration, et al., The Astrophysical Journal 918.2 (2021): 78.
- [7] Healpix, <https://healpix.sourceforge.io/>.
- [8] IceCube Collaboration data release, <https://icecube.wisc.edu/data-releases/2018/07/icecube-catalog-of-alert-events-up-through-icecube-170922a/>.
- [9] TevCat catalog, <http://tevcat.uchicago.edu/>.

Full Authors List: Super-Kamiokande Collaboration

K. Abe^{1,46}, C. Bronner¹, Y. Hayato^{1,46}, K. Hiraide^{1,46}, K. Hosokawa¹, K. Ieki^{1,46}, M. Ikeda^{1,46}, J. Kameda^{1,46}, Y. Kanemura¹, R. Kaneshima¹, Y. Kashiwagi¹, Y. Kataoka^{1,46}, S. Miki¹, S. Mine^{1,6}, M. Miura^{1,46}, S. Moriyama^{1,46}, Y. Nakano¹, M. Nakahata^{1,46}, S. Nakayama^{1,46}, Y. Noguchi¹, K. Sato¹, H. Sekiya^{1,46}, H. Shiba¹, K. Shimizu¹, M. Shiozawa^{1,46}, Y. Sonoda¹, Y. Suzuki¹, A. Takeda^{1,46}, Y. Takemoto^{1,46}, H. Tanaka^{1,46}, T. Yano¹, S. Han², T. Kajita^{2,46,22}, K. Okumura^{2,46}, T. Tashiro², T. Tomiya², X. Wang², S. Yoshida², P. Fernandez³, L. Labarga³, N. Ospina³, B. Zaldivar³, B. W. Pointon^{5,49}, E. Kearns^{4,46}, J. L. Raaf⁴, L. Wan⁴, T. Wester⁴, J. Bian⁶, N. J. Griskevich⁶, S. Locke⁶, M. B. Smy^{6,46}, H. W. Sobel^{6,46}, V. Takhistov^{6,24}, A. Yankelevich⁶, J. Hill⁷, S. H. Lee⁸, D. H. Moon⁸, R. G. Park⁸, B. Bodur⁹, K. Scholberg^{9,24}, C. W. Walter^{9,24}, A. Beauchêne¹⁰, O. Drapier¹⁰, A. Giampaolo¹⁰, Th. A. Mueller¹⁰, A. D. Santos¹⁰, P. Paganini¹⁰, B. Quilain¹⁰, T. Nakamura¹¹, J. S. Jang¹², L. N. Machado¹³, J. G. Learned¹⁴, K. Choi¹⁵, N. Iovine¹⁵, S. Cao¹⁶, L. H. V. Anthony¹⁷, D. Martin¹⁷, N. W. Prouse¹⁷, M. Scott¹⁷, A. A. Sztuc¹⁷, Y. Uchida¹⁷, V. Berardi¹⁸, M. G. Catanesi¹⁸, E. Radicioni¹⁸, N. F. Calabria¹⁹, A. Langella¹⁹, G. De Rosa¹⁹, G. Collazuoli²⁰, F. Iacob²⁰, M. Mattiazzi²⁰, L. Ludovici²¹, M. Gonin²², G. Pronost²², C. Fujisawa²³, Y. Maekawa²³, Y. Nishimura²³, R. Okazaki²³, R. Akutsu²⁴, M. Friend²⁴, T. Hasegawa²⁴, T. Ishida²⁴, T. Kobayashi²⁴, M. Jakkapu²⁴, T. Matsubara²⁴, T. Nakadaira²⁴, K. Nakamura^{24,46}, Y. Oyama²⁴, K. Sakashita²⁴, T. Sekiguchi²⁴, T. Tsukamoto²⁴, N. Bhuiyan²⁵, G. T. Burton²⁵, F. Di Lodovico²⁵, J. Gao²⁵, A. Goldsack²⁵, T. Katori²⁵, J. Migenda²⁵, Z. Xie²⁵, S. Zsoldos^{25,46}, A. T. Suzuki²⁶, Y. Takagi²⁶, Y. Takeuchi^{26,46}, J. Feng²⁷, L. Feng²⁷, J. R. Hu²⁷, Z. Hu²⁷, T. Kikawa²⁷, M. Mori²⁷, T. Nakaya^{27,46}, R. A. Wendell^{27,46}, K. Yasutome²⁷, S. J. Jenkins²⁸, N. McCauley²⁸, P. Mehta²⁸, A. Tarant²⁸, Y. Fukuda²⁹, Y. Ito^{30,31}, H. Menjo³⁰, K. Ninomiya³⁰, J. Lagoda³², S. M. Lakshmi³², M. Mandal³², P. Mijakowski³², Y. S. Prabhu³², J. Zalipska³², M. Jia³³, J. Jiang³³, C. K. Jung³³, M. J. Wilking³³, C. Yanagisawa^{33,*}, M. Harada³⁴, Y. Hino³⁴, H. Ishino³⁴, Y. Koshio^{34,46}, F. Nakanishi³⁴, S. Sakai³⁴, T. Tada³⁴, T. Tano³⁴, T. Ishizuka³⁵, G. Barr³⁶, D. Barrow³⁶, L. Cook^{36,46}, S. Samani³⁶, D. Wark^{36,41}, A. Holin³⁷, F. Nova³⁷, B. S. Yang³⁸, J. Y. Yang³⁸, J. E. P. Fannon³⁹, L. Kneale³⁹, M. Malek³⁹, J. M. McElwee³⁹, M. D. Thiesse³⁹, L. F. Thompson³⁹, S. T. Wilson³⁹, H. Okazawa⁴⁰, S. B. Kim⁴², E. Kwon⁴², J. W. Seo⁴², I. Yu⁴², A. K. Ichikawa⁴³, K. D. Nakamura⁴³, S. Taira⁴³, K. Nishijima⁴⁴, A. Eguchi⁴⁵, K. Nakagiri⁴⁵, Y. Nakajima^{45,46}, S. Shima⁴⁵, N. Taniuchi⁴⁵, E. Watanabe⁴⁵, M. Yokoyama^{45,46}, P. de Perio⁴⁶, S. Fujita⁴⁶, K. Martens⁴⁶, K. M. Tsui⁴⁶, M. R. Vagins^{46,6}, J. Xia⁴⁶, S. Izumiya⁴⁷, M. Kuze⁴⁷, R. Matsumoto⁴⁷, M. Ishitsuka⁴⁸, H. Ito⁴⁸, Y. Ommura⁴⁸, N. Shigeta⁴⁸, M. Shinoki⁴⁸, K. Yamauchi⁴⁸, T. Yoshida⁴⁸, R. Gaur⁴⁹, V. Gousy-Leblanc^{49,†}, M. Hartz⁴⁹, A. Konaka⁴⁹, X. Li⁴⁹, S. Chen⁵⁰, B. D. Xu⁵⁰, B. Zhang⁵⁰, M. Posiadala-Zezula⁵¹, S. B. Boyd⁵², R. Edwards⁵², D. Hadley⁵², M. Nicholson⁵², M. O'Flaherty⁵², B. Richards⁵², A. Ali^{53,49}, B. Jamieson⁵³, S. Amanai⁵⁴, Ll. Marti⁵⁴, A. Minamino⁵⁴ and S. Suzuki⁵⁴

¹Kamioka Observatory, Institute for Cosmic Ray Research, University of Tokyo, Kamioka, Gifu 506-1205, Japan. ²Research Center for Cosmic Neutrinos, Institute for Cosmic Ray Research, University of Tokyo, Kashiwa, Chiba 277-8582, Japan. ³Department of Theoretical Physics, University Autonoma Madrid, 28049 Madrid, Spain. ⁴Department of Physics, Boston University, Boston, MA 02215, USA. ⁵Department of Physics, British Columbia Institute of Technology, Burnaby, BC, V5G 3H2, Canada. ⁶Department of Physics and Astronomy, University of California, Irvine, Irvine, CA 92697-4575, USA. ⁷Department of Physics, California State University, Dominguez Hills, Carson, CA 90747, USA. ⁸Institute for Universe and Elementary Particles, Chonnam National University, Gwangju 61186, Korea. ⁹Department of Physics, Duke University, Durham NC 27708, USA. ¹⁰Ecole Polytechnique, IN2P3-CNRS, Laboratoire Leprince-Ringuet, F-91120 Palaiseau, France. ¹¹Department of Physics, Gifu University, Gifu, Gifu 501-1193, Japan. ¹²GIST College, Gwangju Institute of Science and Technology, Gwangju 500-712, Korea. ¹³School of Physics and Astronomy, University of Glasgow, Glasgow, Scotland, G12 8QQ, United Kingdom. ¹⁴Department of Physics and Astronomy, University of Hawaii, Honolulu, HI 96822, USA. ¹⁵Center for Underground Physics, Institute for Basic Science (IBS), Daejeon, 34126, Korea. ¹⁶Institute For Interdisciplinary Research in Science and Education, ICISE, Quy Nhon, 55121, Vietnam. ¹⁷Department of Physics, Imperial College London, London, SW7 2AZ, United Kingdom. ¹⁸Dipartimento Interuniversitario di Fisica, INFN Sezione di Bari and Università e Politecnico di Bari, I-70125, Bari, Italy. ¹⁹Dipartimento di Fisica, INFN Sezione di Napoli and Università di Napoli, I-80126, Napoli, Italy. ²⁰Dipartimento di Fisica, INFN Sezione di Padova and Università di Padova, I-35131, Padova, Italy. ²¹INFN Sezione di Roma and Università di Roma "La Sapienza", I-00185, Roma, Italy. ²²ILANCE, CNRS - University of Tokyo International Research Laboratory, Kashiwa, Chiba 277-8582, Japan. ²³Department of Physics, Keio University, Yokohama, Kanagawa, 223-8522, Japan. ²⁴High Energy Accelerator Research Organization (KEK), Tsukuba, Ibaraki 305-0801, Japan. ²⁵Department of Physics, King's College London, London, WC2R 2LS, UK. ²⁶Department of Physics, Kobe University, Kobe, Hyogo 657-8501, Japan. ²⁷Department of Physics, Kyoto University, Kyoto, Kyoto 606-8502, Japan. ²⁸Department of Physics, University of Liverpool, Liverpool, L69 7ZE, United Kingdom. ²⁹Department of Physics, Miyagi University of Education, Sendai, Miyagi 980-0845, Japan. ³⁰Institute for Space-Earth Environmental Research, Nagoya University, Nagoya, Aichi 464-8602, Japan. ³¹Kobayashi-Maskawa Institute for the Origin of Particles and the Universe, Nagoya University, Nagoya, Aichi 464-8602, Japan. ³²National Centre For Nuclear Research, 02-093 Warsaw, Poland. ³³Department of Physics and Astronomy, State University of New York at Stony Brook, NY 11794-3800, USA. ³⁴Department of Physics, Okayama University, Okayama, Okayama 700-8530, Japan. ³⁵Media Communication Center, Osaka Electro-Communication University, Neyagawa, Osaka, 572-8530, Japan. ³⁶Department of Physics, Oxford University, Oxford, OX1 3PU, United Kingdom. ³⁷Rutherford Appleton Laboratory, Harwell, Oxford, OX11 0QX, UK. ³⁸Department of Physics, Seoul National University, Seoul 151-742, Korea. ³⁹Department of Physics and Astronomy, University of Sheffield, S3 7RH, Sheffield, United Kingdom. ⁴⁰Department of Informatics in Social Welfare, Shizuoka University of Welfare, Yaizu, Shizuoka, 425-8611, Japan. ⁴¹STFC, Rutherford Appleton Laboratory, Harwell Oxford, and Daresbury Laboratory, Warrington, OX11 0QX, United Kingdom. ⁴²Department of Physics, Sungkyunkwan University, Suwon 440-746, Korea. ⁴³Department of Physics, Faculty of Science, Tohoku University, Sendai, Miyagi, 980-8578, Japan. ⁴⁴Department of Physics, Tokai University, Hiratsuka, Kanagawa 259-1292, Japan. ⁴⁵Department of Physics, University of Tokyo, Bunkyo, Tokyo 113-0033, Japan.

⁴⁶Kavli Institute for the Physics and Mathematics of the Universe (WPI), The University of Tokyo Institutes for Advanced Study, University of Tokyo, Kashiwa, Chiba 277-8583, Japan. ⁴⁷Department of Physics, Tokyo Institute of Technology, Meguro, Tokyo 152-8551, Japan. ⁴⁸Department of Physics, Faculty of Science and Technology, Tokyo University of Science, Noda, Chiba 278-8510, Japan. ⁴⁹TRIUMF, 4004 Wesbrook Mall, Vancouver, BC, V6T2A3, Canada. ⁵⁰Department of Engineering Physics, Tsinghua University, Beijing, 100084, China. ⁵¹Faculty of Physics, University of Warsaw, Warsaw, 02-093, Poland. ⁵²Department of Physics, University of Warwick, Coventry, CV4 7AL, UK. ⁵³Department of Physics, University of Winnipeg, MB R3J 3L8, Canada. ⁵⁴Department of Physics, Yokohama National University, Yokohama, Kanagawa, 240-8501, Japan.

*also at BMCC/CUNY, Science Department, New York, New York, 1007, USA.

†also at University of Victoria, Department of Physics and Astronomy, PO Box 1700 STN CSC, Victoria, BC V8W 2Y2, Canada.